ASME Journal of Electrochemical Energy Conversion and Storage
Online journal at:
https://asmedigitalcollection.asme.org/electrochemical

Zahid Sarıgöl
Faculty of Engineering,
Department of Chemical Engineering,
Gazi University,
Ankara 06570, Turkey
e-mail: zahid.sarigol@metu.edu.tr

Gülay Özkan[1]
Faculty of Engineering,
Department of Chemical Engineering,
Ankara University,
Ankara 06100, Turkey
e-mail: gozkan@eng.ankara.edu.tr

Göksel Özkan[1]
Faculty of Engineering,
Department of Chemical Engineering,
Gazi University,
Ankara 06570, Turkey
e-mail: gozkan@gazi.edu.tr

Development of Boron-Containing Electrolyte Additive for Lithium-Ion Batteries

In this study, triphenylphosphine boron trifluoride ($BF_3 \cdot PPh_3$) was synthesized to be used as an electrolyte additive in Li/$LiCoO_2$ half-cells. Fourier-transform infrared spectroscopy, X-ray diffraction, nuclear magnetic resonance, and X-ray photoelectron spectroscopy analysis techniques were used to determine the structure and composition of the synthesized substance. The battery performance was investigated by adding certain amounts of $BF_3 \cdot PPh_3$ in 1 M $LiPF_6$-ethylene carbonate/dimethyl carbonate/diethyl carbonate (1:1:1 by volume) electrolyte. CR2032 coin cells were assembled with the electrodes and electrolytes prepared in the laboratory. The electrochemical behaviors of the battery were investigated via cyclic voltammetry and charge–discharge tests. The addition of 0.5 wt% and 1 wt% $BF_3 \cdot PPh_3$ in the electrolyte improved the lithium-ion battery's ionic conductivity and capacity retention. The results show that $BF_3 \cdot PPh_3$ has potential applications in lithium-ion batteries. [DOI: 10.1115/1.4063429]

Keywords: lithium-ion, electrolyte, additive, boron, batteries, novel materials

1 Introduction

Rechargeable batteries, used as advanced electric energy storage devices today, are applied in mobile electronic devices such as mobile phones, digital cameras, and laptop computers due to their better performance and environmental friendliness. Recently, Li-ion batteries have attracted worldwide attention due to their high-power storage capacity, fast and efficient charging, and smaller and lighter weight with a longer cycle life span. In most of these batteries, organic liquid electrolytes are used because of their high ionic conductivity and ability to form stable contact with the electrodes. Using these electrolytes in rechargeable batteries creates several safety issues, such as leakage, flammability, and toxicity. As a result, the applications of conventional rechargeable batteries in emerging technologies, including electric vehicles, are limited. To solve this problem, rechargeable batteries containing additives in the electrolyte are used. These electrolytes have excellent performance in terms of safety, good mechanical properties, and design flexibility for batteries. The way additives improve battery cycle life still needs to be better understood, even though researchers worldwide have published hundreds of papers about it [1]. Electrolyte (salts and solvents) decomposition at high potential and elevated temperature is a potential problem. One or more additives may be added to the electrolyte for various purposes. Most additives are designed to prevent solvent reduction or oxidation by forming a protective film on electrode surfaces.

Functional groups containing boron, fluorine, phosphorus, and sulfur are used as additives to increase the electrochemical performance of electrolytes. Fluorine-containing additives increase the storage capacity and discharge capacity due to the high electron-withdrawing tendency of the C–F bond, while the addition of phosphorus or boron-containing functional groups adds flame retardant effects to the electrolyte [2]. Several chelate-borate complexes were used as electrolyte additives, and it was reported that lithium bis(oxalate)borate (LiBOB) showed the best stability and performance among them [3]. Lithium tetrafluoroborate ($LiBF_4$) as an electrolyte additive to improve the cycling performance of $LiNi_{0.5}Co_{0.2}Mn_{0.3}O_2$/graphite cell is reported by Zue et al. With 1.0 wt% $LiBF_4$ addition into the electrolyte, the capacity retention of the lithium-ion battery (LIB) after 100 cycles was significantly improved from 29.2% to 90.1% in the voltage range of 3.0–4.5 V [4]. Lithium hexafluorophosphate ($LiPF_6$), $LiBF_4$, and LiBOB are commercial lithium salts. All these salts contain either phosphorus or boron. Extensive analysis revealed that electrolytes containing boron and phosphorus contribute to the formation of the solid electrolyte interphase (SEI) [5]. Pyridine-boron trifluoride additives were used by Nie et al. [6]. Chen et al. showed that lithium difluorophosphate (LiDFP) is an additive [7]. Fluorinated phosphate ester is an electrolyte additive that improves battery performance by forming an SEI layer on the cathode surface [8]. Beltrop et al. reported that the discharge capacity and Coulombic efficiency (CE) of graphite/NMC811 cells increased remarkably with the addition of triphenylphosphine oxide to 1 M $LiPF_6$-EC/EMC (3:7 by mass) electrolyte [9]. Xu et al. reported that triphenylphosphine contributes to the formation of a stable SEI on the cathode [10]. Another reason for the deterioration of the electrolyte is the electrochemical reactions (reduction and oxidation) in Li-ion cells at high temperatures and voltages. Impedance increase, depletion of active lithium, and gas evolution arise from the electrolyte decomposition. The study stated that Lewis bases stabilized electrolytes consisting of organic carbonate solvents and $LiPF_6$ against degradation at high temperatures up to 85 °C. Triphenylphosphine is a Lewis base. It has been reported that Lewis bases can reduce the gases formed during the cycle by neutralizing acidic gases such

[1]Corresponding authors.

Manuscript received December 23, 2022; final manuscript received August 11, 2023; published online October 5, 2023. Assoc. Editor: Nianqiang Wu.

as PF_5, hydrofluoric acid (HF), and CO_2, which are released by electrolyte decomposition [11].

In this work, this is the first time, we introduce triphenylphosphine boron trifluoride ($BF_3 \cdot PPh_3$) as an electrolyte additive for the application in Li/$LiCoO_2$ cells. The chemical structure as well as some major general properties of $BF_3 \cdot PPh_3$ is investigated. $BF_3 \cdot PPh_3$ possesses the advantages of low cost, non-toxicity, and greatly improved cell performance. Therefore, it can be concluded that this electrolyte additive is promising for advancing LIBs.

2 Materials and Methods

Triphenylphosphine ($(C_6H_5)_3P$, Sigma-Aldrich, 99%), boron trifluoride diethyl etherate ($BF_3 \cdot Et_2O$, Sigma-Aldrich), and hexane (Sigma-Aldrich, ≥95%) were used in the synthesis of $BF_3 \cdot PPh_3$. $LiPF_6$ (lithium hexafluorophosphate, Acros Organics, 98%), dimethyl carbonate (DMC) (Acros Organics, 99%), diethyl carbonate (DEC) (Sigma-Aldrich, ≥99%), and ethylene carbonate (EC) (Acros Organics, 99%+) were used in electrolyte production. $LiCoO_2$ (Sigma-Aldrich, 99.8%), graphite (AMG, 4–5, 5 μm), carbon black (AMG, 4 μm), polyvinylidene fluoride binder (PVDF, Sigma-Aldrich, pellet), and N-methyl pyrrolidone (NMP, Sigma-Aldrich, ≥99.5%) were used in electrode production. Celgard brand separators were used in battery assembly processes.

Electrode film laying operations were performed on Sheen Instruments Doctor Blade, conductivity measurements were performed on GOnDO Electronic PL-700AL, and weighing operations were performed on Radwag AS 220.R2 instruments. MTI MSK-160E devices were used in battery compression, and MTI MSK-T-10 devices were used in electrode and separator cutting processes. Solartron SI-1287 potentiostat was used for battery galvanostatic charge–discharge tests, and IviumStat.h potentiostat-galvanostat was used for loop voltammetry (CV) tests. The batteries were assembled in MBRAUN LABstar (O_2 and $H_2O < 1$ ppm) glovebox.

2.1 Experimental System. In lithium-ion battery electrolyte doping experiments, $BF_3 \cdot PPh_3$ was synthesized as the additive material. The synthesized substance was added to the 1 M $LiPF_6$-EC/DMC/DEC (1:1:1 by volume) electrolyte in three different ratios. The electrodes of the coin cells, where the performance of the additive material is tested, have been produced according to the literature [12]. Coin cell batteries were assembled with electrolytes doped at different rates. Electrochemical tests of the coin cells with doped and undoped electrolytes were carried out.

2.2 Synthesis and Characterization of $BF_3 \cdot PPh_3$. The $BF_3 \cdot PPh_3$ was synthesized according to the literature [13]. First, 0.525 g (2.00 mmol) PPh_3 was added into a 25 ml flask in an inert medium. By adding 15 ml of hexane, PPh_3 was dissolved, and a clear solution was formed. Then 0.5 ml (4.08 mmol) $BF_3 \cdot Et_2O$, stored in the refrigerator, was added dropwise to the solution with a syringe, and a white cloud was formed immediately. The solution was stirred at room temperature for 1.5 h. The flask, closed under inert gas, was kept in the refrigerator at −20 °C overnight and $BF_3 \cdot PPh_3$ was crystallized. The solution was filtered to separate the solid. Then, the solid was dried after being washed with toluene to obtain 0.5 g of $BF_3 \cdot PPh_3$. (yield: 80% white powder).

2.3 Preparation of Electrolytes. The electrolyte is usually a lithium salt, such as $LiPF_6$, dissolved in an organic solvent. As the standard electrolyte, 1 M $LiPF_6$-EC/DMC/DEC (1:1:1 by volume) was chosen [12]. First, 3.3 ml (4.36 g) of EC, 3.3 ml of DMC, and 3.3 ml of DEC were mixed in a glass bottle. Then, 1.52 g of $LiPF_6$ salt was added to this solution and stirred for 1 h to obtain the standard electrolyte. The standard electrolyte was divided into two and taken into separate containers. The synthesized $BF_3 \cdot PPh_3$ additive material, with different mass ratios with respect to the standard electrolyte, was added to the above solutions under magnetic stirring.

2.4 Preparation of Electrodes. $LiCoO_2$ as the cathode active material and graphite as the anode active material were used. The slurries were prepared from active material (85%), carbon black (7.5%), and PVDF binder (7.5%) dispersed in NMP solvent. The slurries were mixed for 12 h. In the production of cathodes, aluminum foil was used as the current collector, while copper foil was used for anodes. The thin-film coating was applied onto the aluminum foil by doctor blade and dried at 120 °C in a vacuum oven [14]. The obtained electrode sheets were punched with a coin cells disc cutter to get electrode discs with a diameter of 19 mm.

2.5 Coin Cell Assembly. A flowchart of the coin cell construction procedure and coin cell assembly is given in Fig. 1.

The electrode-cutting process and the cell assembly were performed in the glovebox. The electrodes and separators were cut into appropriate sizes using the cutting machine. For the CR2032 coin cell, the separator was cut to 20 mm, and the anode and cathodes prepared in the laboratory were cut in diameters of 19 and 15 mm, respectively. As a result of the electrochemical tests carried out, it was understood that the graphite anode produced in the laboratory was working with low efficiency. Therefore, lithium metal with a diameter of 12 mm was cut to be used as the anode. The batteries were remanufactured using lithium metal as the anode, and all tests were performed with these Li/$LiCoO_2$ batteries.

The cut electrodes were weighed, and the amount of active material was determined. In the cell assembly, first, the cathode was placed on the positive cap. Three drops of electrolyte were added to the cathode. The separator was placed to cover the cathode completely. Another three drops of electrolyte were added to the separator, and the anode was placed over the separator. The spacer was placed on the current collector of the anode, and a spring was placed on it. The cell was sealed with the negative cap and then crimped using the compact crimping machine. The preparation of cells was repeated for each electrolyte with different amounts of additive.

3 Results and Discussion

$BF_3 \cdot PPh_3$ was synthesized with the Eq. (1) [13].

$$(C_6H_5)_3P + BF_3 \cdot O(C_2H_5)_2 \rightarrow (C_6H_5)_3P \cdot BF_3 + (C_2H_5)_2O \quad (1)$$

A white solid powder was obtained with an efficiency of 80%. To observe the characteristic peaks of $BF_3 \cdot PPh_3$, the solid was analyzed by Fourier-transform infrared spectroscopy (FTIR) spectroscopy (Fig. 2).

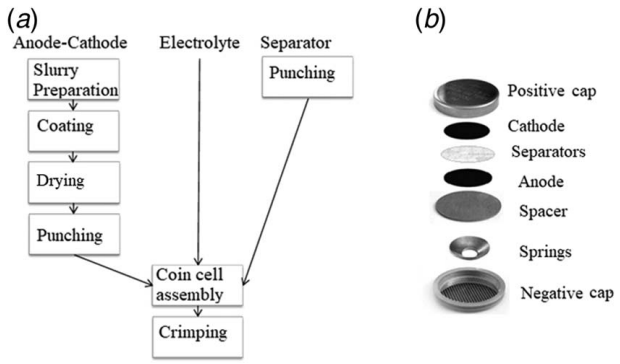

Fig. 1 (*a*) Flowchart of the coin cell construction procedure and (*b*) CR2032 coin-type battery assembly sequence

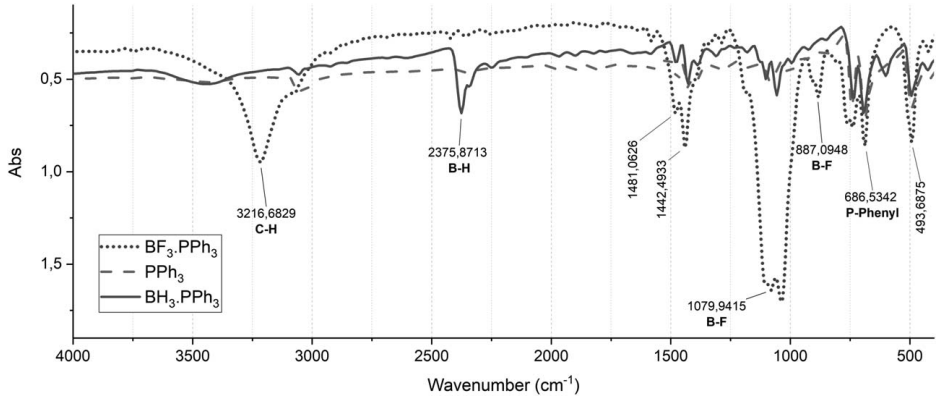

Fig. 2 FTIR results of synthesized $BF_3 \cdot PPh_3$

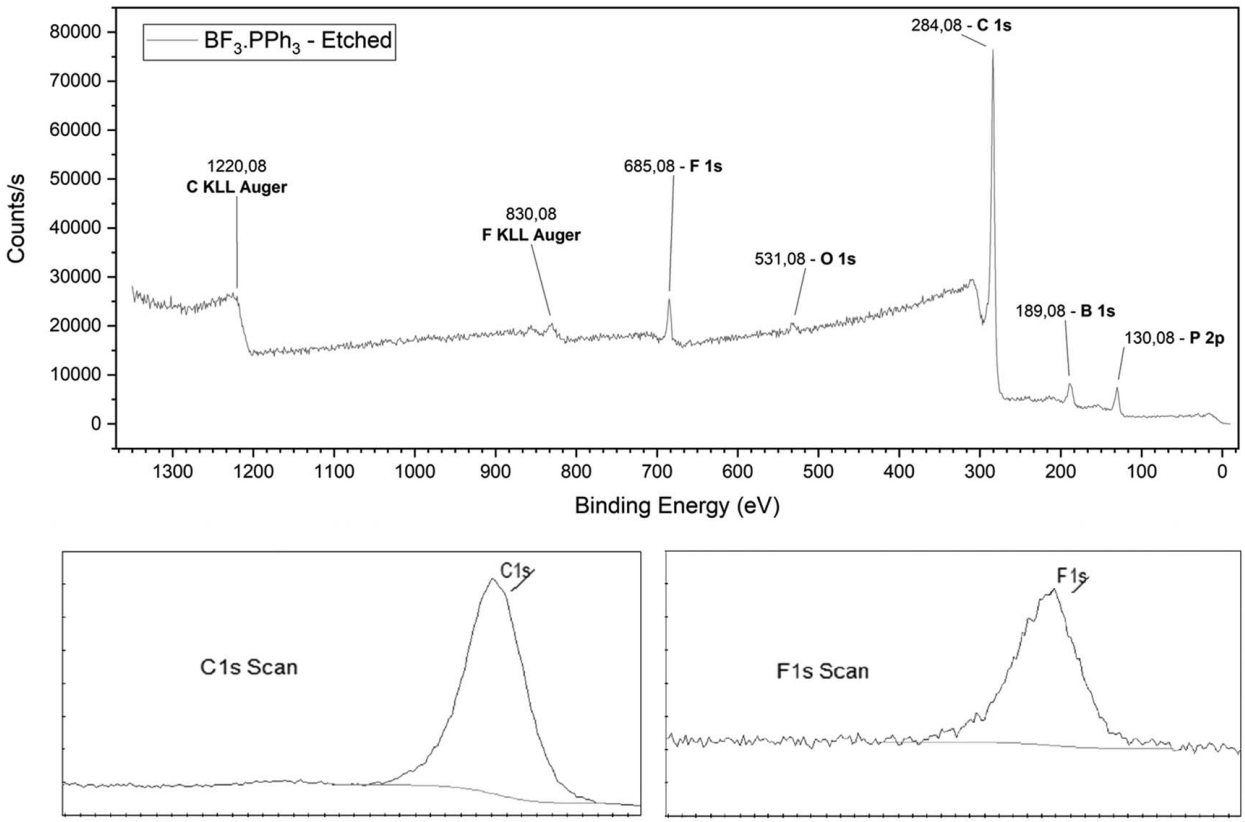

Fig. 3 XPS spectrum of the $BF_3 \cdot PPh_3$

Triphenylphosphine (PPh_3), which is also used in the synthesis of $BF_3 \cdot PPh_3$, was used as a reference substance in the FTIR analysis. PPh_3, shown with a dashed line in Fig. 2, gave the same peaks as $BF_3 \cdot PPh_3$ in the fingerprint region.

In the synthesized $BF_3 \cdot PPh_3$ Infrared (IR) results, the range of 2375–2400 cm^{-1} band (B–H stretching), 1079, and 887 cm^{-1} wavelengths (B–F bending) were noticed. Also, 686 and 3216 cm^{-1} wavelengths P–phenyl bond peaks and C–H stretches were observed, respectively. According to FTIR results, the product matches with previous reports [15].

The X-ray photoelectron spectroscopy (XPS) spectrum of the substance is given in Fig. 3. $BF_3 \cdot PPh_3$ synthesis was carried out in an oxygen-free environment. The weak O 1 s peak at 531 eV was interpreted as sample contamination due to contact with air during analysis. Theoretically, $BF_3 \cdot PPh_3$ ($(C_6H_5)_3P \cdot BF_3$) is

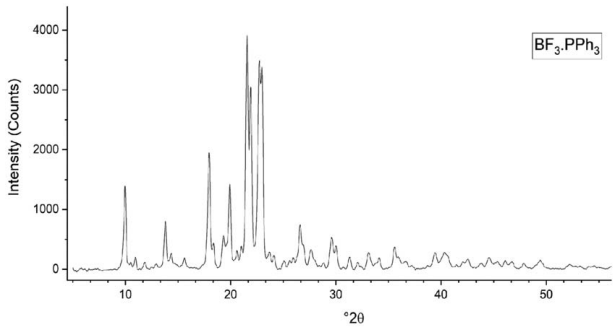

Fig. 4 XRD analysis of the $BF_3 \cdot PPh_3$

Table 1 The overlap ratios of the synthesized substance with the reference substance peaks

Chemical formula	The overlap ratios (%)
$C_{25}H_{22}BF_4P$	82.9
$C_{18}H_{16}B_2F_5OP$	17.1

composed of 65.65% carbon and 17.32% fluorine. The XPS analysis showed that the substance contained 65.56% carbon and 13.52% fluorine.

The X-ray diffraction (XRD) analysis of the $BF_3.PPh_3$ is given in Fig. 4. XRD data of synthesized $BF_3 \cdot PPh_3$ were analyzed using the "Match" program. The XRD patterns of the sample were compared with a database of reference patterns for phase identification. The overlap ratios of the synthesized substance with the reference substance peaks were calculated with reference intensity ratio (RIR), and the result obtained is given in Table 1. RIR is a method used for the quantitative analysis of XRD results. This method compares all diffraction data of the analyzed substance with the diffraction data of standard reference materials.

Table 2 Calculated and theoretical mass percentages of elements in $BF_3 \cdot PPh_3$

	Percent by mass (%)	
Elements	Calculated from XRD results	Theoretical
C	65.88	65.65
F	18.42	17.32
P	7.17	9.42
H	4.87	4.56
B	2.97	3.04
O	0.69	–

The percentages by mass of the elements in the synthesized substance were calculated with the similarity ratios obtained as a result of the comparison with the models. The calculated values were compared with the theoretical mass percent (Table 2). The comparison results were interpreted as the peaks in the XRD analysis belonging to the $BF_3 \cdot PPh_3$ structure. As a result of XRD analysis, it was seen that $BF_3 \cdot PPh_3$ has a triclinic crystal structure.

Upon analysis, it has been noted that the component percentages align well with the theoretical percentages for the expected $BF_3 \cdot PPh_3$ compound. The presence of oxygen in the synthesized compound was due to $BF_3 \cdot Et_2O$ in the synthesis medium and was interpreted as causing a low rate of borate formation in the structure.

The ^{11}B nuclear magnetic resonance (NMR) result of $BF_3 \cdot PPh_3$ is given in Fig. 5. It was observed that it gave a peak at −17.33 ppm. $BF_3 \cdot Et_2O$ peak was observed at 0 ppm. Boron compounds with tetrahedral structures appear to range from −15 ppm to −22 ppm [16]. It was concluded from theFTIR, and ^{11}B NMR results that $BF_3 \cdot PPh_3$ was synthesized at a high purity level.

3.1 Conductivity Results of Electrolyte Solutions. The conductivity values of electrolyte solutions at different temperatures are given in Table 3. As expected, conductivity values increased with increasing temperature.

The ionic conductivity increased with the increase of the doping amount. These values are consistent with the literature [7].

3.2 Galvanostatic Charge–Discharge Test Results. Figure 6(*a*) shows the 47th and 48th cycles of the undoped battery, the 24th cycle of the 0.5 $BF_3 \cdot PPh_3$ doped battery, and the 18th

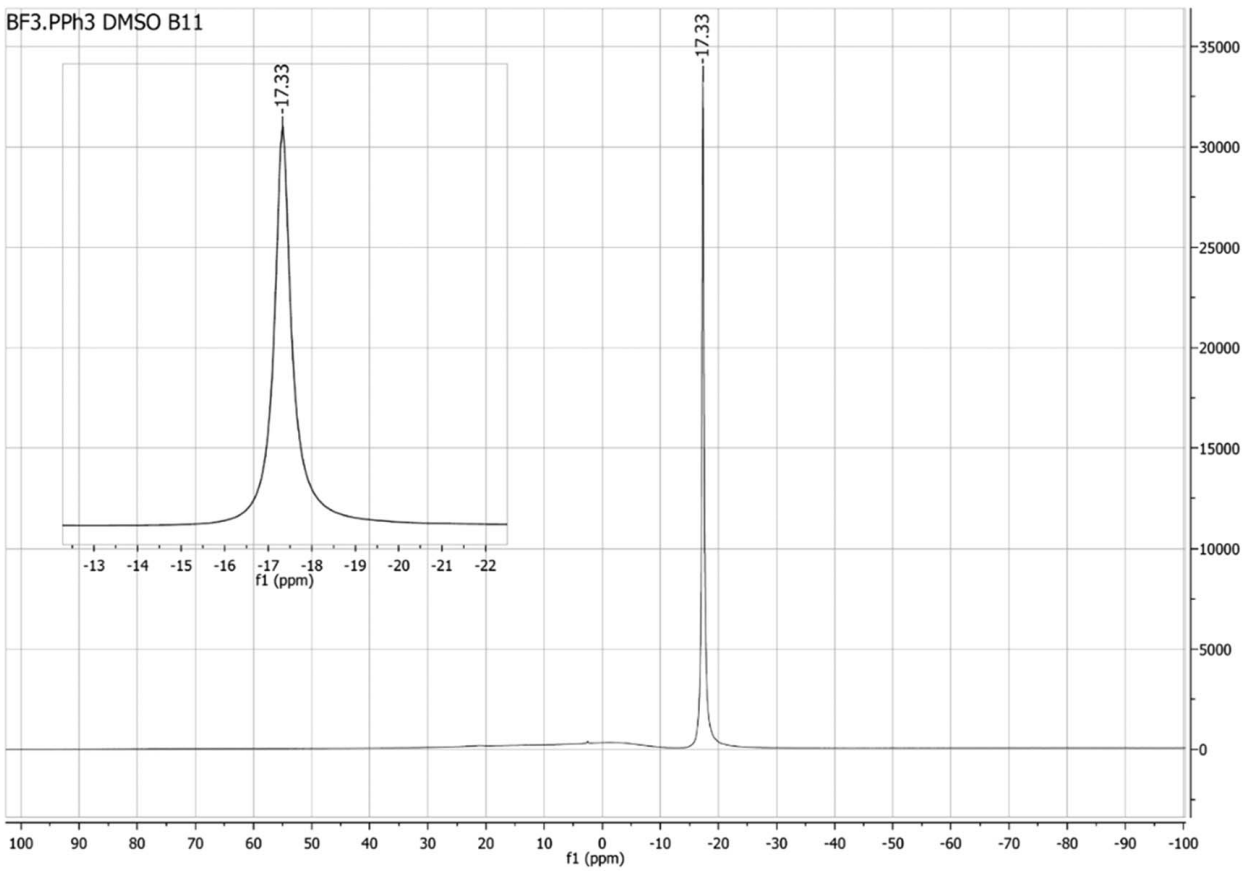

Fig. 5 ^{11}B NMR results of synthesized $BF_3 \cdot PPh_3$

Table 3 Conductivity results of electrolyte solutions at different temperatures

	Conductivity (mS/cm) at 25 °C	Conductivity (mS/cm) at 35 °C	Conductivity (mS/cm) at 45 °C
Without $BF_3 \cdot PPh_3$	8.15	9.22	9.84
0.5 wt% $BF_3 \cdot PPh_3$	8.91	10.04	10.73
1 wt% $BF_3 \cdot PPh_3$	9.08	10.25	10.86

cycle of the 1% $BF_3 \cdot PPh_3$ doped battery. With the increase in doping, the charge and discharge times of the batteries, i.e., the charge and discharge capacities, have increased. In order to compare battery performances, the current values applied to each battery and the active material masses and specific capacities of the batteries must be calculated. This graph shows that for these batteries, whose current values and active material masses are very close to each other, the battery capacity increases as the doping ratio increases. In other words, Fig. 6(*a*) demonstrates that increasing the amount of additive directly correlates with an increase in battery discharge time. Since the current is constant, the longer it takes for the battery to discharge, the higher the discharge capacity. In the figure, having completed fewer cycles means having a larger capacity. An unconventional yet effective way of comparing the capacities of batteries.

3.3 Cycling Performance of the Li/$LiCoO_2$ Cells. Figures 6(*b*) and 6(*c*) display the cyclic performances of Li/$LiCoO_2$ cells according to capacity and Coulombic efficiency. The cell without the additive shows a discharge specific capacity of 24.4 mAh/g after the 50th cycle with 74% CE. In comparison, the capacities of the cells with the 0.5% $BF_3 \cdot PPh_3$ and 1% $BF_3 \cdot PPh3$ additives at the 50th cycle are 40.8 mAh/g (87% CE) and 53.2 mAh/g (above 100% CE), respectively. The cell with the 1%$BF_3 \cdot PPh_3$ can deliver a much higher specific capacity as well as a much higher Coulombic efficiency. It is seen that cells with 0.5 and 1 wt% additive have a Coulombic efficiency above 100% in some cycles. This can be seen in half-cell batteries (one of the electrodes being lithium metal). Since the anode is a Li metal, the Li-ions passing from the anode to the cathode during the discharge of the battery may be more than the incoming Li-ions during charging. Another situation that can cause a Coulombic efficiency above 100% is the charge of the battery before the first charge. In this case, the charge transferred to the battery to reach 4 V may be less than the charge released from the battery for it to drop to 2 V. These two conditions are valid for all batteries with and without additives, and they lose their importance with increased cycles. It should be noted that the cell using 0.5% $BF_3 \cdot PPh_3$ shows poorer cycling stability than the cell using 1% $BF_3 \cdot PPh_3$ (at the 130th cycle, 77.7 mAh/g) (Fig. 6(*d*)). Xu et al. [17] suggested that additives can only be used in a small concentration. Figure 7 shows how the battery capacity changes during discharge. The fact is that the cell shows similar performance with and without $BF_3 \cdot PPh_3$ in the range 4–3.3 V. It has been interpreted that the additive does not contribute to the high potential of the cell.

The d*Q*/d*V* curves of the cells are shown in Fig. 8(*a*) at the 50th cycle. In the charge and discharge curves of the graph, it is seen that all cells show the same performance, up to 3.3 V. The capacity

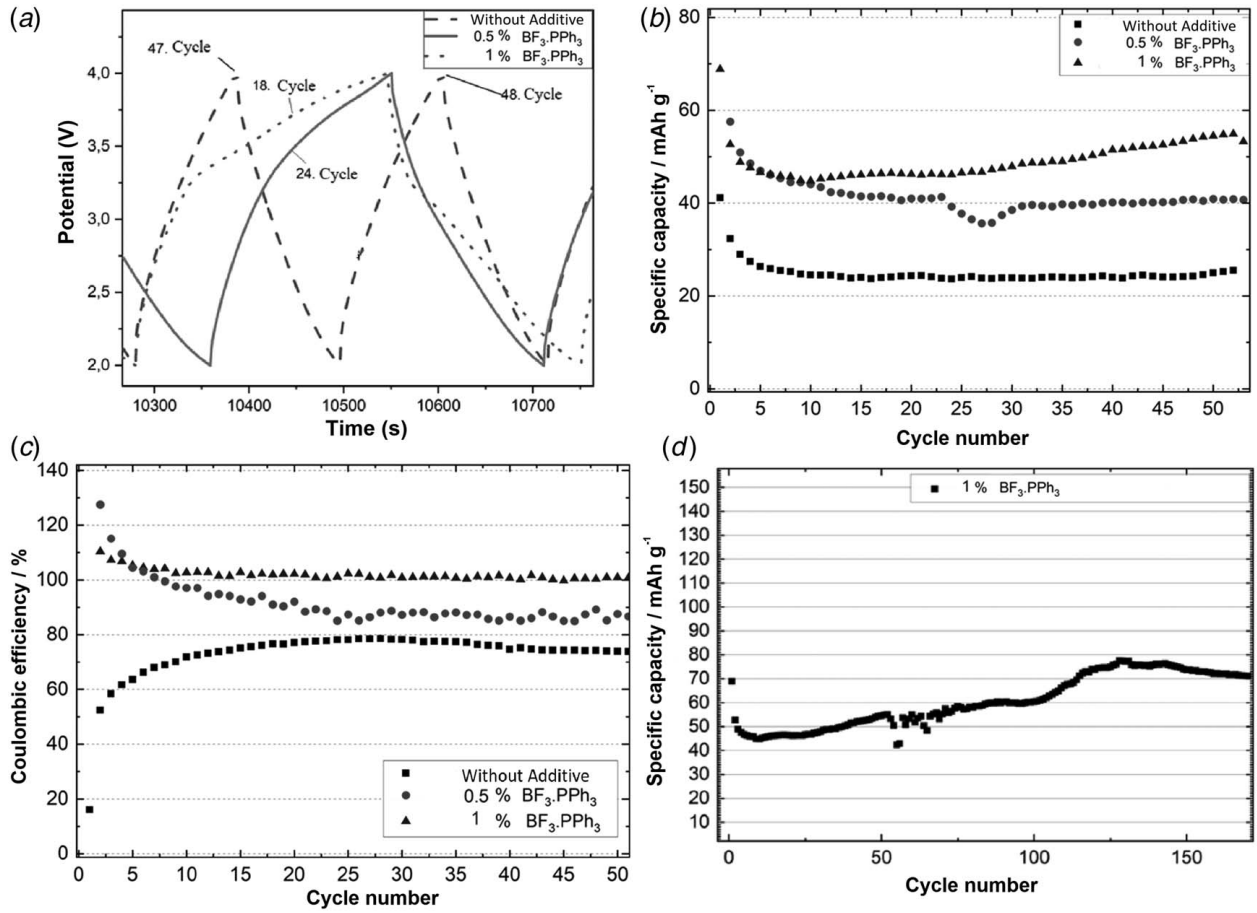

Fig. 6 (*a*) Potential-time graphs of batteries (1250–10,750 s), (*b*) specific discharge capacities, (c) Coulombic efficiencies, and (*d*) specific discharge capacities of the battery with 1% $BF_3 \cdot PPh_3$

difference between with and without $BF_3 \cdot PPh_3$ is mainly due to the charge entering the cell between 2.5 V and 3.5 V.

The dQ/dV analysis can also be used to monitor how the cell changes over time. As the number of cycles of the cell increases, the position, height, and shape of the differential capacitance curves change. In Figs. 8(*a*), 8(*c*), and 8(*d*), the discharge peaks shift to lower voltage values due to the increase in polarization with the increase in the number of cycles. This is a characteristic of lithium-ion batteries. In all cells, the amount of charge released from the battery at 2 V decreases with the increase in the number of cycles. Additive presence leads to increased charge release at high cell potentials the absence of additive results in no such effect.

3.4 Cyclic Voltammograms. The electrochemical behavior of the 1 M $LiPF_6$-EC/DMC/DEC (1:1 by weight without additive,

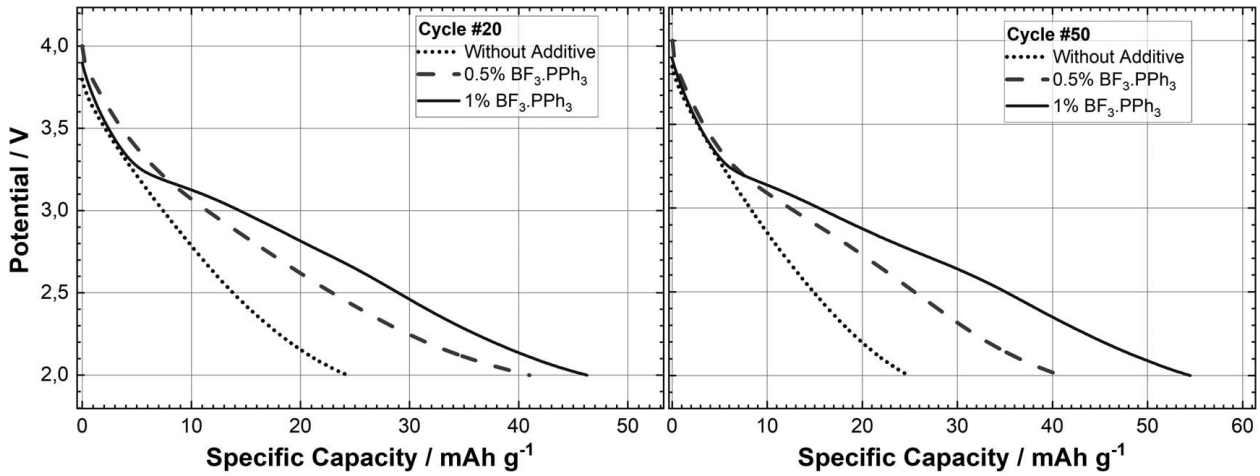

Fig. 7 The 20th and 50th cycle potential—discharge specific capacity graphs of batteries

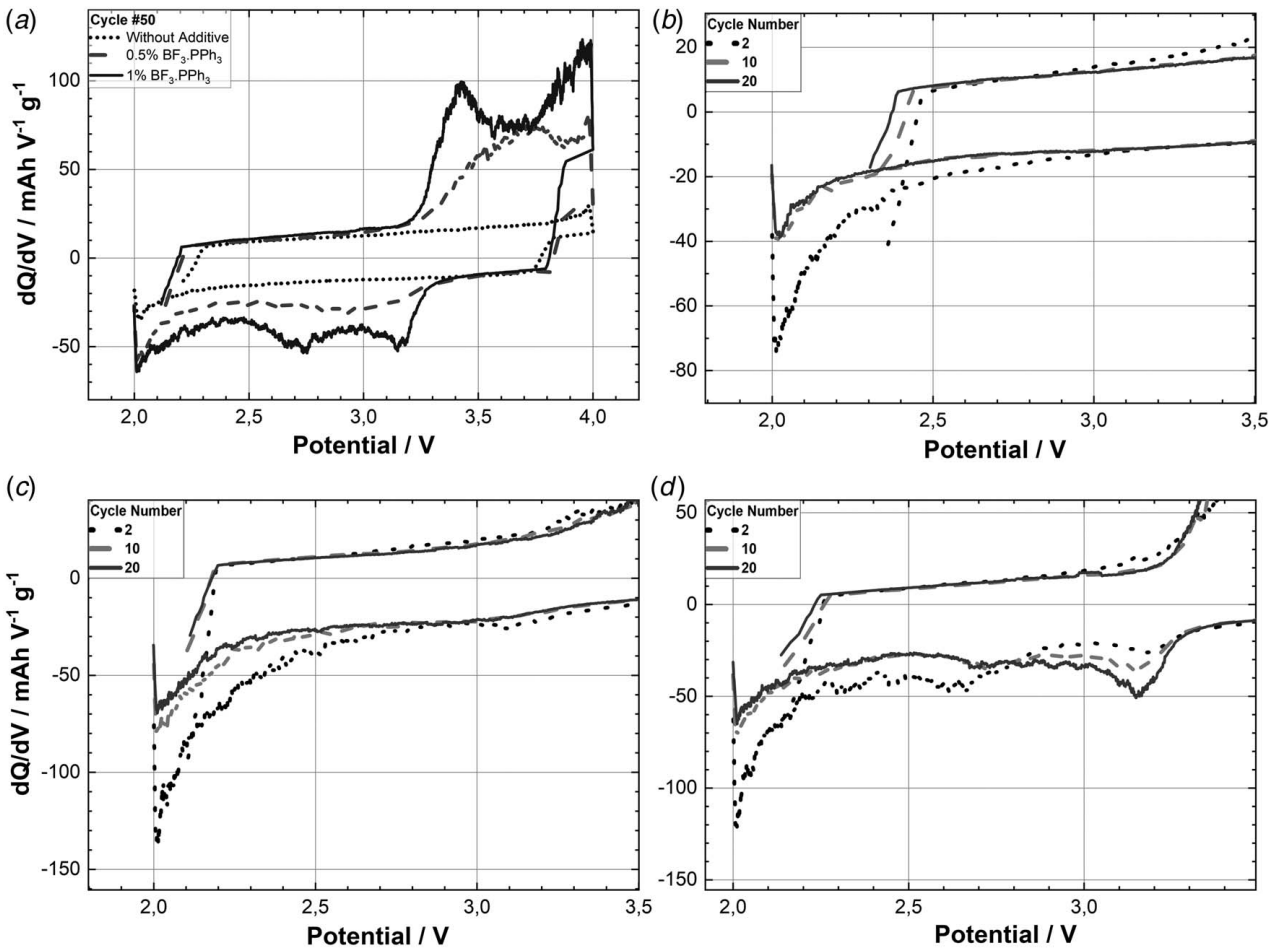

Fig. 8 Differential capacity graphs of batteries: (*a*) after the 50th cycle, (*b*) without additive, (c) 0.5% $BF_3 \cdot PPh_3$, and (*d*) 1% $BF_3 \cdot PPh_3$

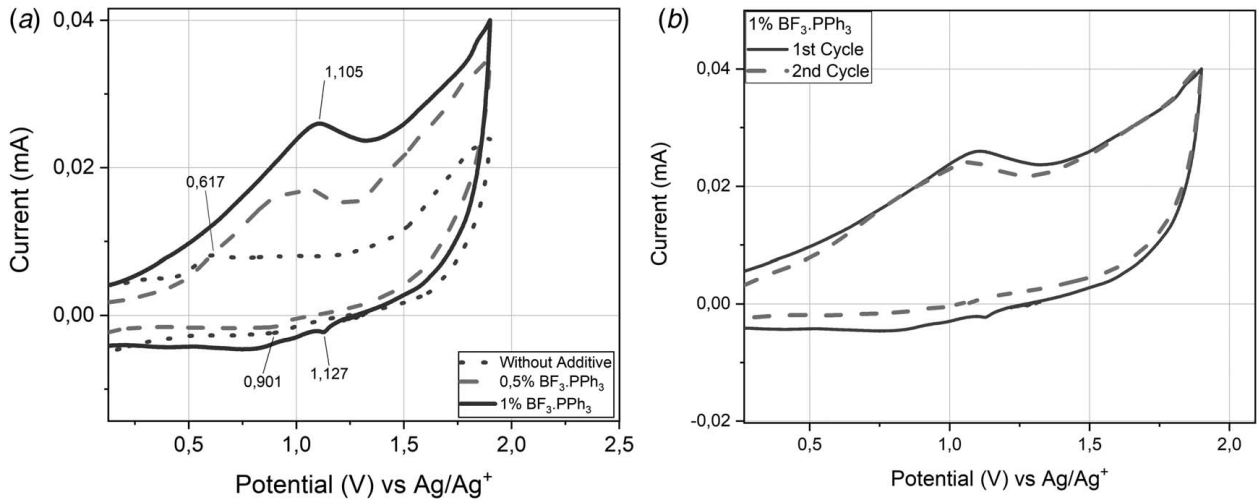

Fig. 9 (*a*) CV measurements of electrolyte without additive, with 0.5 wt% and 1 wt% $BF_3 \cdot PPh_3$ and (*b*) 1st and 2nd CV cycles of the electrolyte with 1 wt% $BF_3 \cdot PPh_3$

with 0.5% $BF_3 \cdot PPh_3$, with 1% $BF_3 \cdot PPh_3$) electrolytes were investigated with potentiostat-galvanostat (IviumStat.h). Glassy carbon was used as the working electrode, and platinum wire was used as the counter electrode. Tests were performed using an anhydrous Ag/Ag^+ reference electrode in an argon gas environment between −2 V and 1.9 V at a scan rate of 50 mV/s. The results are presented in Fig. 9(*a*). The reduction peaks of 0%, 0.5%, and 1% $BF_3 \cdot PPh_3$ doped (1 M $LiPF_6$-EC/DMC/DEC) electrolytes were detected at potentials of 0.9 V (peak overlaid by EC-decomposition peak), 0.9, and 1.1 V (reduction of $BF_3 \cdot PPh_3$), respectively. This was interpreted as the additive reduced at higher potentials than the standard electrolyte; thus, the additive reduces the reduction of the main electrolyte components.

Figure 9(*b*) shows that the reduction peak around 0.9 and 1.1 V decreased in the second cycle of the electrolyte doped with 1 wt% $BF_3 \cdot PPh_3$ because of the formation of an SEI layer in the first cycle. This layer improves battery performance by preventing further reduction of the electrolyte in later cycles [3].

4 Conclusions

The development of electrolyte additives to improve the performance of lithium-ion batteries without significantly changing the production process has been the subject of research for many years. In this study, it was aimed to develop a boron-containing electrolyte additive. $BF_3 \cdot PPh_3$ was successfully synthesized as an electrolyte additive for $Li/LiCO_2$ cells. Cyclic voltammetry and charge–discharge tests were carried out to examine the electrochemical performance of the batteries. It was observed that certain properties of batteries containing 0.5 and 1 wt% $BF_3 \cdot PPh_3$ doped electrolytes were improved compared to the battery containing standard electrolytes. The specific discharge capacity of the battery with 0.5 wt% additive was measured 67% more than the reference battery after the first 50 cycles, at cycles between 2 and 4 V. It was observed that the Coulombic and voltaic efficiencies of the doped batteries are increased. The results obtained from cyclic voltammetry suggest that doping may indeed have a significant impact on the formation of the solid electrolyte interface. It was found that doping did not contribute to the high-voltage operation of the batteries. Experimental results show that $BF_3 \cdot PPh_3$ has an application area as an electrolyte additive in lithium-ion batteries.

Conflict of Interest

There are no conflicts of interest.

Data Availability Statement

The authors attest that all data for this study are included in the paper.

References

[1] Song, W. T., Gauthier, R., Taskovic, T., Ouyang, D. X., Ingham, H. A., Eldesoky, A., Azam, S. M., et al., 2022, "Lithium Difluoro (Dioxalato) Phosphate as an Electrolyte Additive for NMC811/Graphite Li-Ion Pouch Cells," J. Electrochem. Soc., **169**(11), p. 110513.

[2] Reddy, T., and Linden, D., 2010, *Linden's Handbook of Batteries*, 4th ed., McGraw-Hill Professional Publishing, New York, pp. 540–550.

[3] Kaymaksiz, S., Wilhelm, F., Wachtler, M., Wohlfahrt-Mehrens, M., Hartnig, C., Tschernych, I., and Wietelmann, U., 2013, "Electrochemical Stability of Lithium Salicylatoborates as Electrolyte Additives in Li-Ion Batteries," J. Power Sources, **239**, pp. 659–669.

[4] Zuo, X., Fan, C., Liu, J., Xiao, X., Wu, J., and Nan, J., 2013, "Lithium Tetrafluoroborate as an Electrolyte Additive to Improve the High Voltage Performance of Lithium-Ion Battery," J. Electrochem. Soc., **160**(8), pp. 1199–1204.

[5] Zhang, S., 2010, "Fluorohaloborate Salts, Synthesis and Use Thereof (United States Patent No. 7,833,660 B1), US Patent and Trademark Office.

[6] Nie, M., Xia, J., and Dahn, J. R., 2015, "Development of Pyridine-Boron Trifluoride Electrolyte Additives for Lithium-Ion Batteries," J. Electrochem. Soc., **162**(7), pp. 1186–1195.

[7] Chen, H., Liu, B., Wang, Y., Guan, H., and Zhou, H., 2021, "Insight Into Wide Temperature Electrolyte Based on Lithiumdifluoro (Oxalate) Borate for High Voltage Lithium-Ion Batteries," J. Alloys Compd., **876**, pp. 159966–159970.

[8] Tan, S., Zhang, Z., Li, Y., Li, Y., Zheng, J., Zhou, Z., and Yang, Y., 2013, "Tris(Hexafluoro-Iso-Propyl)Phosphate as an SEI-Forming Additive on Improving the Electrochemical Performance of the Li[Li 0.2 Mn 0.56 Ni 0.16 Co 0.08]O_2 Cathode Material," J. Electrochem. Soc., **160**(2), pp. 285–292.

[9] Beltrop, K., Klein, S., Nölle, R., Wilken, A., Lee, J. J., Köster, T. K.-J., Reiter, J., et al., 2018, "Triphenylphosphine Oxide as Highly Effective Electrolyte Additive for Graphite/NMC811 Lithium Ion Cells," Chem. Mater., **30**(8), pp. 2726–2741.

[10] Xu, J., Hu, Y., Liu, T., and Wu, X., 2014, "Improvement of Cycle Stability for High-Voltage Lithium-Ion Batteries by In-Situ Growth of SEI Film on Cathode," Nano Energy, **5**, pp. 67–73.

[11] Tasaki, K., Kanda, K., Nakamura, S., and Ue, M., 2003, "Decomposition of $LiPF_6$ and Stability of PF_5 in Li-Ion Battery Electrolytes. Density Functional Theory and Molecular Dynamics Studies," J. Electrochem. Soc., **150**(12), pp. 1628–1636.

[12] Wang, X., Xue, W., Hu, K., Li, Y., Li, Y., and Huang, R., 2018, "Adiponitrile as Lithium-Ion Battery Electrolyte Additive: A Positive and Peculiar Effect on High-Voltage Systems," ACS Appl. Energy Mater., **1**(10), pp. 5347–5354.

[13] Burke, J. M., 2002, "Structural Studies of Novel Molecular Systems," Doctoral Dissertation, Durham University, Durham, UK, pp. 109–120.

[14] Kayyar, A., Huang, J., Samiee, M., and Luo, J., 2012, "Construction and Testing of Coin Cells of Lithium Ion Batteries," J. Visual. Exp., **66**, p. 4104.

[15] Beg, M. A. A., and Clark, H. C., 2011, "Chemistry of the Trifluoromethyl Group: Part V. Infrared Spectra of Some Phosphorus Compounds Containing CF_3," Can. J. Chem., **40**(3), pp. 393–398.

[16] Nöth, H., and Wrackmeyer, B., 1978, "Tables of 11B-NMR Data," *Nuclear Magnetic Resonance Spectroscopy of Boron Compounds*, H. Nöth, and B. Wrackmeyer, eds., Springer, Berlin/Heidelberg, Germany, pp. 109–429.

[17] Xu, M., Liu, Y., Li, B., Li, W., Li, X., and Hu, S., 2012, "Tris (Pentafluorophenyl) Phosphine: An Electrolyte Additive for High Voltage Li-Ion Batteries," Electrochem. Commun., **18**, pp. 123–126.